







PAPER

[View Article Online](#)
[View Journal](#) | [View Issue](#)Cite this: *Nanoscale Adv.*, 2020, 2, 4242

Nickel sulfide-incorporated sulfur-doped graphitic carbon nitride nanohybrid interface for non-enzymatic electrochemical sensing of glucose†

S. Vinoth, ^{ac} P. Mary Rajaitha, ^a A. Venkadesh, ^b K. S. Shalini Devi, ^a
S. Radhakrishnan ^b and A. Pandikumar ^{*ac}

A nickel sulfide-incorporated sulfur-doped graphitic carbon nitride (NiS/S-g-C₃N₄) nanohybrid was utilized as an interface material for the non-enzymatic sensing of glucose in an alkaline medium (0.1 M NaOH). The precursors used in the preparation of NiS/S-g-C₃N₄ hybrid were thiourea and nickel nitrate hexahydrate as the sulfur and nickel sources, respectively. The HRTEM results reveal that NiS nanoparticles incorporated on the S-g-C₃N₄ nanosheet surface could enhance the electrocatalytic activity and electrical conductivity. The prepared NiS/S-g-C₃N₄ crystalline nature, surface functionalities, graphitic nature, thermal stability and surface composition were investigated using XRD, FT-IR, Raman spectroscopy, TGA and XPS analyses. The NiS/S-g-C₃N₄ modified electrode was used for the non-enzymatic sensing of glucose at an applied potential of 0.55 V vs. Ag/AgCl with a detection limit of 1.5 μM (S/N = 3), sensitivity of 80 μA mM⁻¹ cm⁻² and the response time of the fabricated sensor was close to 5 s. Different inorganic ions and organic substances did not interfere during glucose sensing. The NiS/S-g-C₃N₄ nanohybrid material could be extended for a real sample analysis and open the way for diverse opportunities in the electrochemical sensing of glucose.

Received 1st March 2020

Accepted 30th July 2020

DOI: 10.1039/d0na00172d

rsc.li/nanoscale-advances

1. Introduction

Glucose sensing has profound importance in the field of clinical diagnostics, biotechnology, environmental monitoring, pharmaceutical analysis and food production.^{1,2} The advanced testing and analyses of glucose levels in blood and urine samples are key markers to identify diabetics that has an increased rate of mortality next to cancer. Until now, the determination of glucose has been carried out by several methods, including fluorescence³ and optical spectroscopy,⁴ acoustic techniques,⁵ surface plasmon resonance spectroscopy,⁶ electrochemiluminescence,⁷ and electrochemical techniques.^{1,8} The advantage of electrochemical methods over other techniques is that they are compact, relatively inexpensive, reliable, sensitive and can achieve real-time analysis. In general, glucose detection mostly involves enzymatic reactions,⁹ but the use of enzyme (glucose oxidase) based biosensor are limited due to the instability of the enzyme activity, expensive fabrication

cost, change of temperature, pH, and half shelf life. Even though commercial sensing devices are inferior to enzymatic systems, the last decade has seen growth in the research interest in non-enzymatic glucose sensing with different nanomaterials. The advances in nanotechnology have enabled new possibilities for making modernistic glucose sensors with non-enzymatic methods. The poor selectivity and surface fouling problem could be solved with electrocatalyst nanostructure-based non-enzymatic sensors and exhibit higher sensitivity compared with enzymatic systems.¹⁰

Glucose enzymatic biosensors require different modification strategies such as the electropolymerization of enzyme,¹¹ cross-linking of enzyme,¹² enzyme entrapping by sol-gel methods,¹³ wiring enzyme electrodes of glucose oxidase to electrochemically mediated polymer chains,¹⁴ etc., to achieve stability. These efforts confirmed the stability of enzymatic glucose sensors for short-term period and facilitate one-time usage only. The enzymatic glucose sensor based on glucose oxidase is exposed to thermal and chemical conditions during modification, storage and usage. To overcome these limitations, non-enzymatic sensors based on the glucose oxidation reaction and catalysed by various electrocatalysts such as noble metal nanoparticles,¹⁵ transition metal oxides,^{16–18} carbon nanotubes,¹⁹ gold nanocages,²⁰ polymer composites,¹¹ alloys,²¹ complexes,^{22–24} Ni₃S₂/NiMoO₄ nanowires,²⁵ Ag-/Au-NiCo₂O₄ nanosheets,²⁶ NiO hollow cages,²⁷ porous NiCo₂O₄ nanoarrays,²⁸ and Ni/Al layered double hydroxides,²⁹ have been employed.

^aElectro Organic and Materials Electrochemistry Division, CSIR-Central Electrochemical Research Institute, Karaikudi-630 003, Tamil Nadu, India. E-mail: pandikumarinbox@gmail.com; pandikumar@cecri.res.in

^bElectrode and Electrocatalysis Division, CSIR-Central Electrochemical Research Institute, Karaikudi-630 003, Tamil Nadu, India

^cAcademy of Scientific and Innovative Research (AcSIR), Ghaziabad-201002, India

† Electronic supplementary information (ESI) available. See DOI: 10.1039/d0na00172d



Niu *et al.* investigated non-enzymatic glucose sensing with three-dimensional porous nickel nanostructures with a low detection limit of $0.07\ \mu\text{M}$.³⁰ Huo *et al.* reported non-enzymatic glucose detection using 3D- Ni_3S_2 nanosheet arrays supported on Ni foam with high electrocatalytic activity towards glucose detection, $1.2\ \mu\text{M}$, with a high sensitivity of $6148.0\ \mu\text{A}\ \text{mM}^{-1}\ \text{cm}^{-2}$.³¹ The polymeric semiconductor, graphitic carbon nitride ($\text{g-C}_3\text{N}_4$), has recently acquired research interest in the area of electrochemical sensors due to its extensive unique properties. To increase the electrocatalytic activity and electrical conductivity, sulfur-based $\text{g-C}_3\text{N}_4$ has been tuned for quick electron transfer.²² Further, Tian *et al.* analyzed ultrathin graphitic carbon nitride nanosheets utilized as highly efficient electrocatalyst materials for glucose biosensing with a limit of detection and linear range of $11\ \mu\text{M}$ and $1\text{--}12\ \text{mM}$, respectively.³² Kim *et al.* reported nickel sulfide nanostructures for non-enzymatic glucose sensing with a limit of detection of $0.82\ \mu\text{M}$.³³ Also, to avoid the inactivation of analyte in the reaction solutions, various metal-based glucose sensors have been exploited. Along with these metals chalcogenides, the redox chemistry of transition metal chalcogenides (TMCs) has demonstrated higher activity of glucose oxidation due to its layer-dependent physical and chemical properties, which can enhance the redox activity.³⁴ Among various TMCs, nickel sulfide (NiS) has been widely used as an electrode interface material for the non-enzymatic detection of glucose due to its high conductivity, but its use in electrochemical sensors for any analyte in combination with S- $\text{g-C}_3\text{N}_4$ has not been explored to date. Kim *et al.* reported morphology-controlled Ni_3S_2 utilized for non-enzymatic glucose sensors with a $0.82\ \mu\text{M}$ limit of detection.³³ The $\text{g-C}_3\text{N}_4$ electrochemical sensing activity was limited due to the surface fouling, chemical inertness and poor conductivity. Hence, the electrochemical performance of $\text{g-C}_3\text{N}_4$ could be enhanced by hybridization with other nanomaterials applied in the fabrication of electrochemical sensors.^{35,36} Functionalized $\text{g-C}_3\text{N}_4$ and its hybrid/composite materials have been employed for the electrochemical detection of glucose, nitrobenzene,

H_2O_2 , NADH, and mercuric ions.^{37–39} Moreover, Sun and co-workers investigated the $\text{g-C}_3\text{N}_4$ nanosheets utilized in electrochemical glucose bio-sensing with an $11\ \mu\text{M}$ LoD in buffer solution.³⁸ In addition, $\text{g-C}_3\text{N}_4$ nanosheets have been exploited with the enzymatic oxidation of glucose using glucose oxidase.⁴⁰ Kannan *et al.* investigated the glucose oxidation through fabrication of NiS thin films used for a non-enzymatic glucose sensor with a $0.32\ \mu\text{M}$ LoD and response time of $<8\ \text{s}$.⁴¹ Hence, in this work, the NiS/S- $\text{g-C}_3\text{N}_4$ nanohybrid material was fabricated as the interface matrix and explored as an electrode material for glucose oxidation (Scheme 1) and the electrochemical parameters were investigated.

2. Experimental methods

2.1. Chemicals and reagents

Chemicals such as thiourea ($\text{CH}_4\text{N}_2\text{S}$) and nickel nitrate hexahydrate ($\text{Ni}(\text{NO}_3)_2 \cdot 6\text{H}_2\text{O}$) were purchased from SRL laboratories and used as received. All other reagents were of analytical grade and used without further purification. Double distilled water was utilized throughout the experiments, which was collected from a MILLIPORE water system.

2.2. Synthesis of NiS-incorporated S- $\text{g-C}_3\text{N}_4$ nanosheets

The NiS-incorporated S- $\text{g-C}_3\text{N}_4$ nanosheets were synthesized by the following procedure (Scheme 1A). First, 3 g of thiourea with 600 mg of nickel nitrate hexahydrate were mixed in an agate mortar and pestle for an hour. The resulting mixture was transferred to an alumina crucible for calcination at $550\ ^\circ\text{C}$ for 3 h. It was then allowed to cool down to room temperature in order to obtain NiS-engulfed S-doped $\text{g-C}_3\text{N}_4$. The bare S- $\text{g-C}_3\text{N}_4$ was prepared by the same procedure without the addition of nickel nitrate hexahydrate. The prepared samples were denoted as NiS/S- $\text{g-C}_3\text{N}_4$ and S- $\text{g-C}_3\text{N}_4$, respectively.

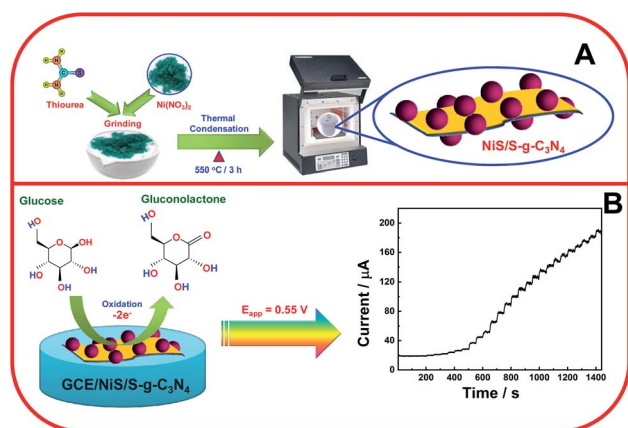
2.3. Fabrication of the NiS/S- $\text{g-C}_3\text{N}_4$ /GCE nanohybrid

The modified glassy carbon electrode (GCE) was fabricated by dispersing 1 mg of the NiS/S- $\text{g-C}_3\text{N}_4$ in 1 mL distilled water and $5\ \mu\text{L}$ of the solution was drop-casted onto a glassy carbon electrode (GCE) and allowed to dry at room temperature. The modified GCE was used as a working electrode and it was designated as NiS/S- $\text{g-C}_3\text{N}_4$ /GCE.

3. Results and discussion

3.1. Morphological studies of S- $\text{g-C}_3\text{N}_4$ -NiS nanohybrid materials

The HRTEM images of NiS/S- $\text{g-C}_3\text{N}_4$ are shown in Fig. 1(A and B). The NiS nanoparticles were randomly incorporated into S- $\text{g-C}_3\text{N}_4$ nanosheet layers. HRTEM results obviously reveal the interfacial contacts between NiS and S- $\text{g-C}_3\text{N}_4$, which promote the charge transfer and increase the active sites of the catalyst, thus improving the electrocatalytic activity and electrical conductivity during glucose sensing. In addition, High Angle Annular Dark Field – Scanning Transmission Electron Microscopy (HAADF-STEM) images confirm the presence of individual



Scheme 1 (A) Schematics for the synthesis of the NiS/S- $\text{g-C}_3\text{N}_4$ nanohybrid material and (B) schematics for the electrocatalytic oxidation of glucose at the NiS/S- $\text{g-C}_3\text{N}_4$ modified electrode and its electrochemical response.



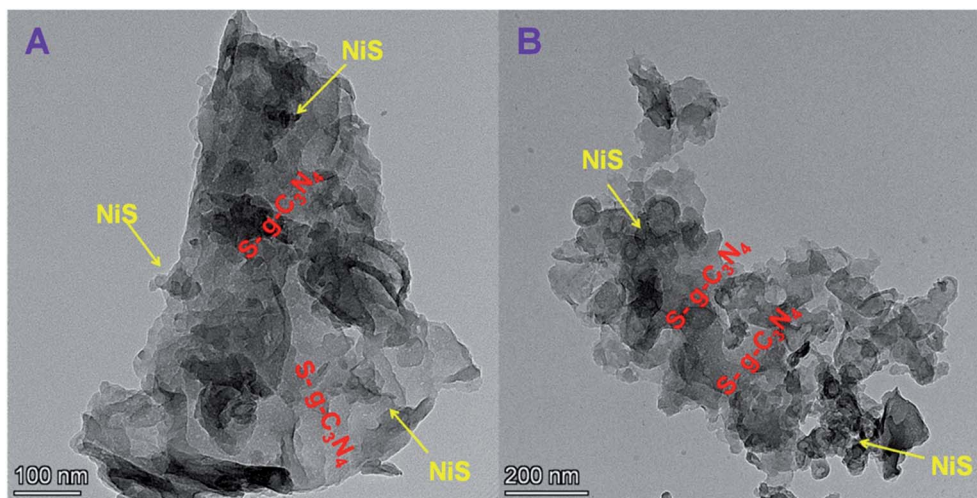


Fig. 1 (A and B) HRTEM images obtained for the NiS/S-g-C₃N₄ nanohybrid material.

elements such as Ni, S, C and N in the NiS/S-g-C₃N₄ nanohybrid materials (Fig. 2(A–F)).

3.2. FT-IR and Raman spectral studies of NiS/S-g-C₃N₄ nanohybrid material

The surface functionalities and chemical bonding in the prepared samples were investigated by FT-IR spectroscopy, as shown in Fig. 3(A). The integration of NiS in S-g-C₃N₄ did not significantly alter the FT-IR spectrum of S-g-C₃N₄. However, the reduction in the spectrum intensity is said to be due to the integration of NiS in the NiS/S-g-C₃N₄ nanohybrid material. In both materials, the FT-IR signal observed in 1200 to 1650 cm^{−1} could be attributed to the stretching vibrations of heptazine heterocyclic (C₆N₇) units of S-g-C₃N₄.⁴² The peak at 810 cm^{−1} is due to the breathing vibration of triazine units, which is due to

the condensed CN heterocycles.⁴³ The bands from 2900 to 3500 cm^{−1} were attributed to the adsorbed water molecules and N–H vibration of the uncondensed amine groups. The presence of these bonds was found in the NiS/S-g-C₃N₄ nanohybrid material with low intensity due to the integration of NiS, which induced the change in the chemical bonding. However, NiS/S-g-C₃N₄ exhibits a peak at 617 cm^{−1}, due to the Ni–S stretching vibration mode of NiS.⁴⁴ The FT-IR spectra of bulk g-C₃N₄, g-C₃N₄ nanosheets, S-g-C₃N₄, and NiS/S-g-C₃N₄ are shown in Fig. S1.† There is no significant change in the triazine and heptazine units in the g-C₃N₄ polymeric network. However, the intensity variation represents the nature of the chemical bonding in the different g-C₃N₄ structures. The corresponding Raman spectra exhibited in Fig. S2† show the G band and D band; thus, the graphitic nature of the carbon nitride family

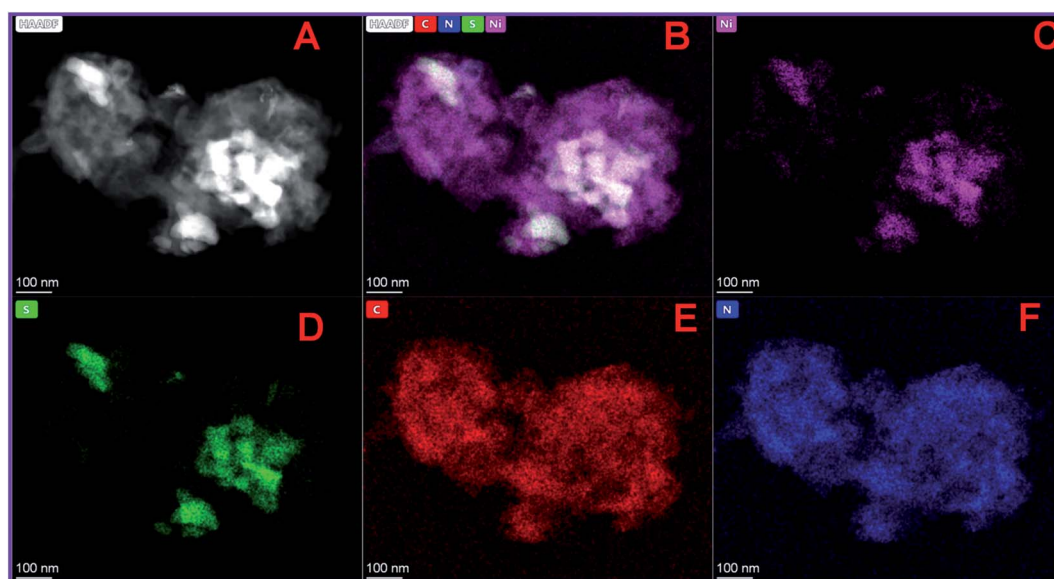


Fig. 2 (A and B) HAADF-STEM image and elemental mapping of (C) Ni, (D) S, (E) C and (F) N in NiS/S-gC₃N₄ nanohybrid materials.



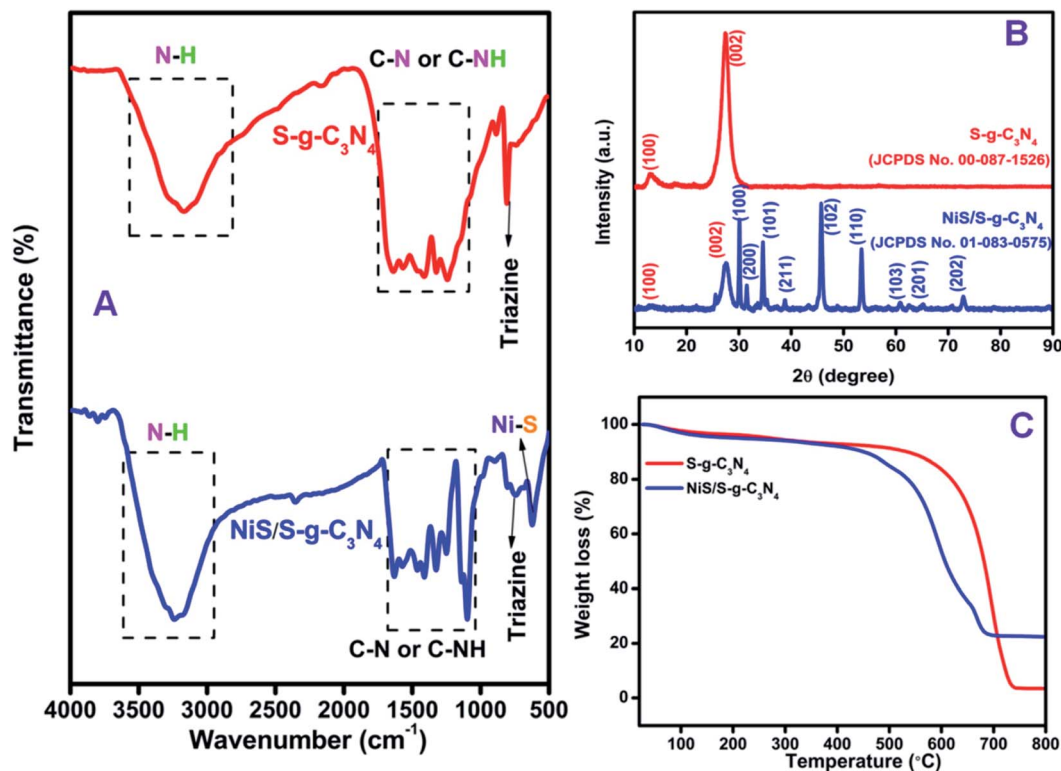


Fig. 3 (A) FT-IR spectra, (B) XRD patterns and (C) TGA curves obtained for S-g-C₃N₄ and the NiS/S-g-C₃N₄ nanohybrid material.

could be confirmed in the bulk g-C₃N₄, g-C₃N₄ nanosheets, S-g-C₃N₄, and NiS/S-g-C₃N₄ samples.

3.3. X-ray diffraction analysis of NiS/S-g-C₃N₄ nanohybrid materials

The X-ray diffraction (XRD) pattern of the S-g-C₃N₄ and NiS/S-g-C₃N₄ nanohybrid material was studied to confirm the crystalline phase and the obtained results are shown in Fig. 3(B). The XRD pattern of S-g-C₃N₄ shows two main peaks at 2θ values of 13.3° and 27.5°, corresponding to the (100) and (002) planes, respectively;⁴⁵ thus, the patterns are in good agreement with JCPDS card no: 00-087-1526. The peak at 27.5° appears due to the interlayer stacking of conjugated aromatic systems and the peak at 13.3° is due to the in-plane structural packing of aromatic systems.⁴⁶ The XRD pattern of the NiS/S-g-C₃N₄ nanohybrid material shows peaks at 13.3° and 27.5°, corresponding to the (100) and (002) planes, respectively, due to the presence of S-g-C₃N₄ in the hybrid material. The other peaks at 30.2°, 31.7°, 34.7°, 39.3°, 45.9°, 53.6°, 60.5°, 65.1°, and 73.0° correspond to the (100), (200), (101), (211), (102), (110), (103), (201), and (202) planes due to the existence of NiS in the NiS/S-g-C₃N₄ nanohybrid material, respectively, and these peaks match well with JCPDS card no: 01-083-0575.

3.4. Thermo-gravimetric analysis of NiS/S-g-C₃N₄ nanohybrid material

The thermal stability and the composition of the prepared sample was studied using the thermo-gravimetric analysis

(TGA) curves obtained at a heating rate of 10 °C min⁻¹ under air atmosphere from room temperature to 800 °C. As shown in Fig. 3(C), the NiS/S-g-C₃N₄ nanohybrid material decomposes at lower temperatures compared with pure S-g-C₃N₄. When the increase in temperature is over 700 °C, the S-g-C₃N₄ undergoes complete decomposition. The combustion temperature of the nanohybrid material is reduced due to the presence of embedded NiS particles in the S-g-C₃N₄.

3.5. X-ray photoelectron spectroscopy studies of the NiS/S-g-C₃N₄ nanohybrid material

The surface composition and oxidation states of the elements in NiS/S-g-C₃N₄ were confirmed by X-ray photoelectron spectroscopic (XPS) analysis and the results shown in Fig. 4. The survey scan for the NiS/S-g-C₃N₄ nanohybrid material reveals the presence of C, N, Ni and S (Fig. 4(A)). The C 1s core-level spectrum (Fig. 4(B)) was deconvoluted into three peaks at 285.7, 284.8 and 282.2 eV, which correspond to N=C-N, in which sp² bonded, C-O species on the g-C₃N₄ surface, and C-C are present in the g-C₃N₄ surface, respectively.⁴⁷⁻⁴⁹ The deconvoluted peaks for the N 1s core-level spectrum (Fig. 4(C)) are due to the presence of triazine rings C=N-C (403.2 eV), tertiary nitrogen N-(C)₃ (405.3 eV) and amino functional groups (C-N-H) (407.3 eV), respectively.⁵⁰ Fig. 4(D) shows peaks at 860.5 and 862.4 eV in the Ni 2p spectrum, which are associated with Ni 2p_{3/2} and its satellite peak, and the peaks at 880.2 and 867.7 eV correspond to Ni 2p_{1/2} and its satellite peak⁵¹ in NiS/S-g-C₃N₄. The S 2p spectrum in Fig. 4(E) shows four main peaks at 160.0, 161.5, 163.1 and 165.4 eV. The peaks at 161.5 and 163.1 eV are attributed to



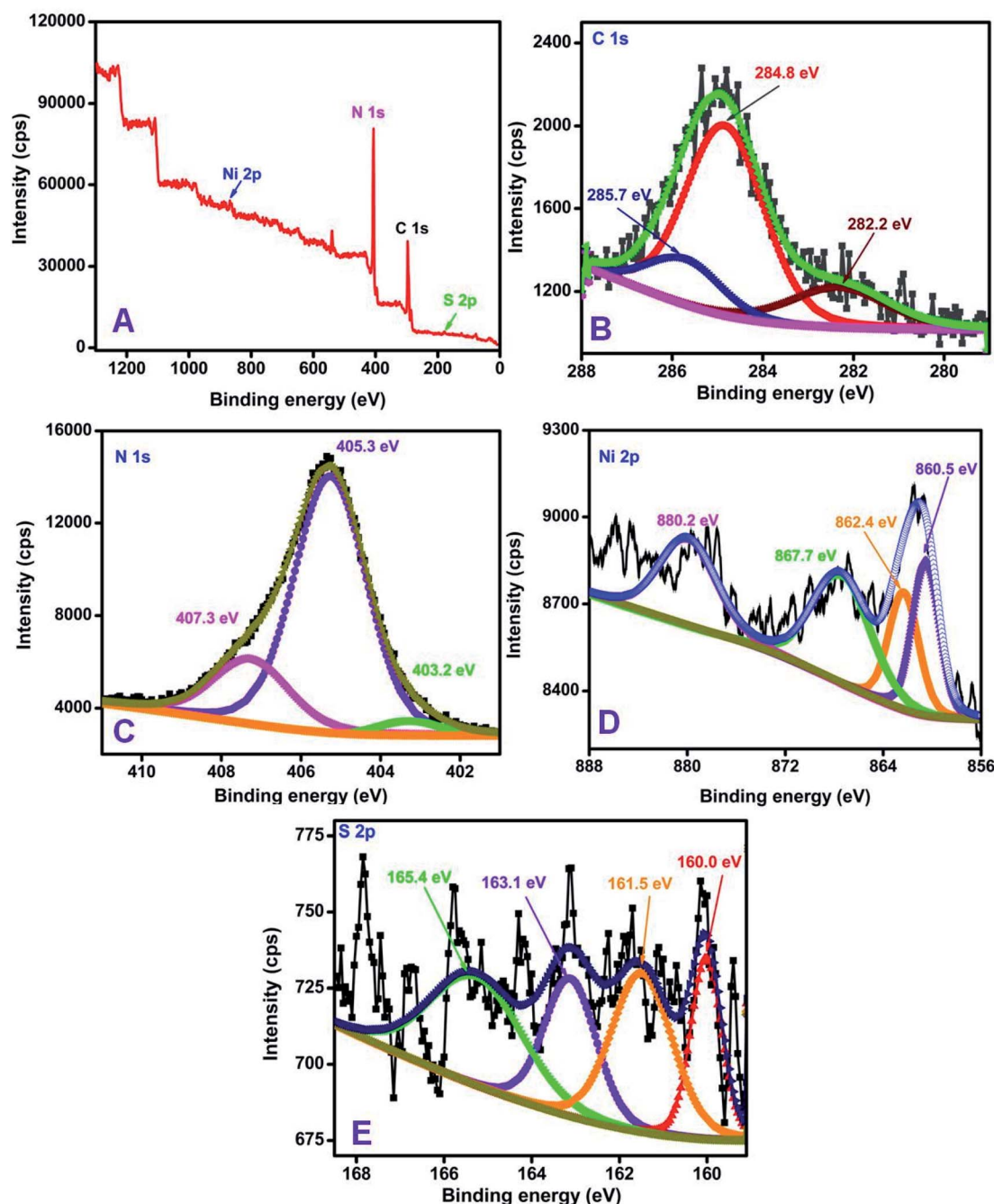


Fig. 4 XPS spectra of the NiS/S-g-C₃N₄ nanohybrid material (A) survey scan, (B) C 1s, (C) N 1s, (D) Ni 2p, and (E) S 2p core-level spectra.

the 2p_{3/2} and 2p_{1/2} of thiophene-S (–C–S–C–) due to spin-orbit coupling, while the peaks at 160.0 eV and 165.4 eV associated with S 2p_{1/2} and S 2p_{3/2}, respectively, are consistent with the S 2p of NiS in NiS/S-g-C₃N₄.⁵² The XPS survey scan for S-g-C₃N₄ and its corresponding C 1s, N 1s and S 2p core-level spectra are shown in Fig. S3† for comparison.

3.6. Electrochemical studies of the NiS/S-g-C₃N₄/GCE modified electrode

Prior to the electrochemical measurements, the electrode-dependent properties of the modified electrode were

compared with the benchmark ferricyanide (Fe(CN)₆^{3–/4–}) system in the potential window of –0.2 V to +0.8 V vs. Ag/AgCl (Fig. 5). The redox peak response of bare GCE at –0.2 V vs. Ag/AgCl corresponds to the oxidation/reduction process of the 1 mM Fe(CN)₆^{3–/4–} in 0.1 M KCl solution. On modifying the bare electrode with S-g-C₃N₄, deviation in the peak current and a distorted peak potential were observed, which shows the limited electron transfer behavior of the modified S-g-C₃N₄. To increase and facilitate the electron transfer behavior of the modified electrode, the NiS-incorporated S-g-C₃N₄ nanohybrid material was chosen as an electrode modifier and the redox



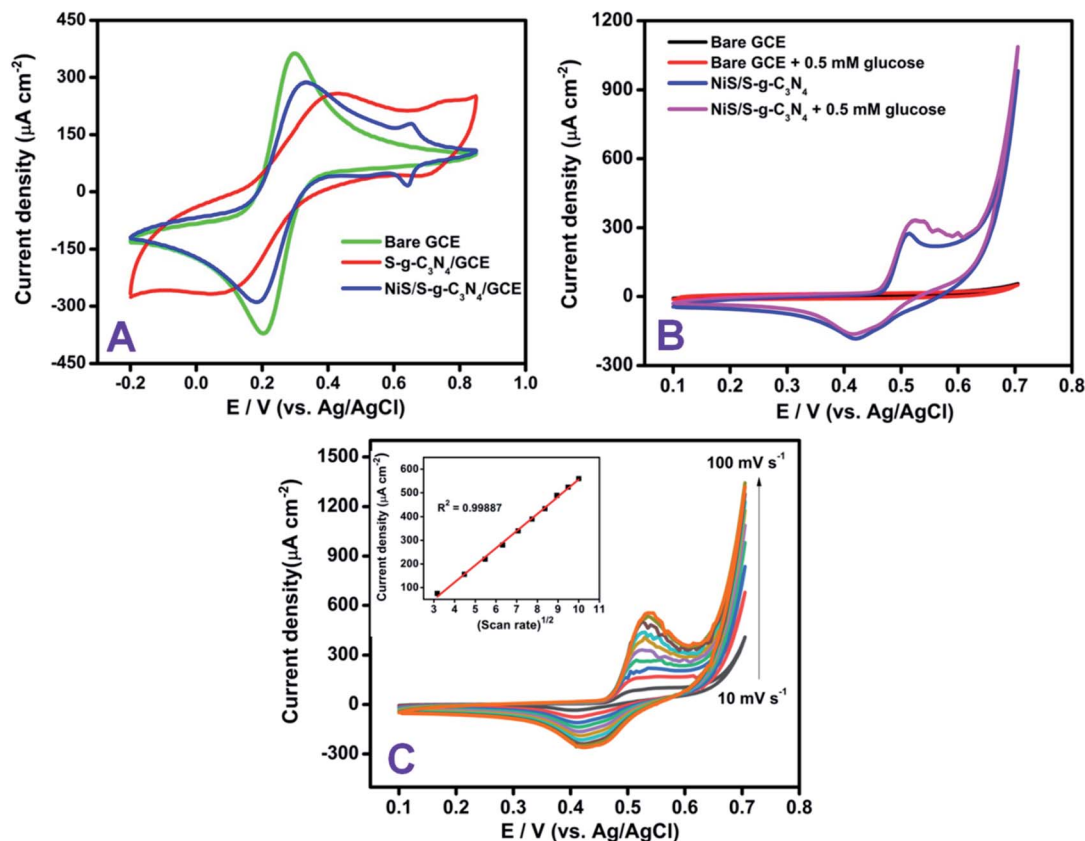


Fig. 5 (A) Comparative CV responses of bare GCE, S-g-C₃N₄/GCE, and NiS/S-g-C₃N₄/GCE in 5 mM K₃[Fe(CN)₆] in 0.5 M KCl solution, (B) comparative CVs of step by step modification of bare GCE, bare GCE with 0.5 mM of glucose, NiS/S-g-C₃N₄ modified GCE and NiS/S-g-C₃N₄ modified GCE with 0.5 mM of glucose in 0.1 M NaOH solution at a scan rate of 50 mV s^{−1} and (C) CV responses of different scan rates (10–100 mV s^{−1}) with 0.5 mM glucose at the NiS/S-g-C₃N₄ modified GCE in 0.1 M NaOH solution. Inset: plot of anodic (*i*_{pa}) and cathodic peak current (*i*_{pc}) vs. scan rate were obtained for 0.5 mM glucose at NiS/S-g-C₃N₄ modified GCE in 0.1 M NaOH solution.

response in the ferricyanide solution shows a defined peak at +0.2 V as well as an additional peak corresponding to nickel sulfide at +0.65 V vs. Ag/AgCl with an *i*_{pa} and peak to peak separation value of 285 μA cm^{−2} and 90 mV, respectively. The influence of electrolyte pH on glucose oxidation was studied for the NiS/S-g-C₃N₄ modified electrode using cyclic voltammetry. Starting from acidic pH 3 to neutral pH, the glucose response was negligible whereas, the modified system exhibited higher oxidation at higher pH 8–11, which showed the NiS interface oxidized the glucose at its maximum only in an alkaline medium. Hence, 0.1 M NaOH was used as the supporting electrolyte throughout the experiments. In addition, different loadings of material (0.5, 1.0, and 1.5 mg mL^{−1}) were monitored for the NiS/S-g-C₃N₄ nanohybrid modified system. The glucose oxidation response was found to increase for the loading of NiS/S-g-C₃N₄ up to 1 mg mL^{−1} whereas, a decrease in the oxidation current was observed in the higher loading concentration of 1.5 mg mL^{−1} of g-C₃N₄ (Fig. S5†).

In order to verify the electrocatalytic performance of the NiS/S-g-C₃N₄ nanohybrid material, CV measurements were recorded in 0.1 M NaOH solution containing 0.5 mM glucose, as shown in Fig. 5(B). The unmodified GCE did not show any appreciable electrocatalytic response. The significant peak current due to

glucose oxidation was observed upon bare GC/NiS modification (Fig. S6†) whereas, the NiS/S-g-C₃N₄ modified GCE showed a greater anodic peak current response after the addition of 0.5 mM glucose in the NaOH solution.

This clearly indicates that the NiS/S-g-C₃N₄ modified electrode has good electrocatalytic performance towards the electro-oxidation of glucose in alkaline medium. Kim *et al.* reported nickel sulfide as an electrocatalyst material for non-enzymatic glucose sensing.³³ Sonkar *et al.* investigated non-enzymatic electrochemical sensing based on nickel complex-immobilized multiwall carbon nanotubes for glucose determination.⁵³ The effect of scan rate was studied for NiS/S-g-C₃N₄/GCE by varying the scan rates ranging from 10 to 100 mV s^{−1} in Fe(CN)₆^{3−/4−} dissolved in 0.1 M KCl as a supporting electrolyte. The oxidation and reduction peak currents of the modified electrode linearly increased by varying different applied scan rates on the electrode surface. The dual peak at +0.2 V and +0.65 V vs. Ag/AgCl were found to linearly trend with the respective scan rates, as shown in Fig. S4,† indicating that the Fe(CN)₆^{3−/4−} redox couple is a diffusion-controlled process at NiS/S-g-C₃N₄/GCE. The regression coefficient was calculated to be *R*² = 0.9998. The dependence of the peak current (*I*_p) and potential (*E*_p) with the scan rate (*v*) were then taken into account to analyze the glucose



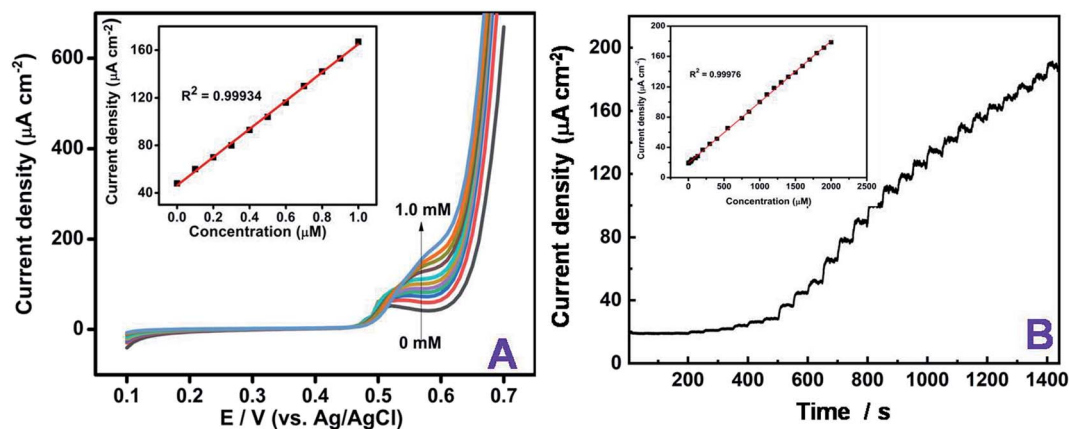


Fig. 6 (A) LSV responses of NiS/S-g-C₃N₄/GCE in 0.1 M NaOH solution at a scan rate of 10 mV s⁻¹ with different concentrations of glucose (0 to 1 mM); inset: calibration plot between current density vs. glucose concentration and (B) amperometric *J*-*T* response of NiS/S-g-C₃N₄ modified GCE upon spiking with sequential additions of 100 μM glucose in 0.1 M NaOH at 0.55 V vs. Ag/AgCl.

oxidation in 0.1 M NaOH as a supporting electrolyte. The addition of 0.5 mM glucose with different scan rates ranging from 10–100 mV s⁻¹ was plotted in the inset of Fig. 5(C), which exhibits the diffusion-controlled electron transfer nature of the electrode. The obtained slope value, being greater than the theoretically expected value of 0.5 for a reversible process, suggests that the electrocatalytic oxidation of glucose can achieve the maximum. To show the steep increase in the concentration of glucose, linear sweep voltammetry was used. The linear increase in the oxidation current was obtained by each addition of increasing concentration glucose from 0 to 1 mM Fig. 6(A). From the slope value, the sensitivity was found to be 118 μA mM⁻¹ cm⁻² and the *R*² value was 0.9993, which confirms the linear response of the modification.

Based on the above findings from cyclic voltammetry experiments, the typical amperometric responses of the NiS/S-g-C₃N₄ modified GCE with the successive addition of glucose in the concentration ranges from 1 to 2100 μM were investigated

and the results obtained are plotted in Fig. 6(B). A stepwise oxidation in the peak current with respect to increasing concentrations of glucose was observed, which in turn acts as a sensitive non-enzymatic glucose sensor with good linear range up to the concentration of 2.1 mM. The limit of quantification (LOQ) was calculated to be 1 μM. The NiS/S-g-C₃N₄ also exhibited a high sensitivity of 80 μA mM⁻¹ cm⁻² and the response time of the fabricated sensor was the average of the stepwise increment from the amperometric *I*-*t* curve during the glucose addition and the calibration plot between the steady state current density vs. glucose concentration, which was close to 5 s. The developed sensor showed an excellent detection of glucose even at low concentrations with a limit of detection (LOD) of 1.5 μM (S/N = 3). From the amperometric *I*-*t* curve, the diffusion coefficient was calculated by the following Cottrell equation,⁵⁴

$$i = nFAD^{1/2}c/\pi^{1/2}t^{1/2} \quad (1)$$

Table 1 Various modified electrodes and their analytical performance in non-enzymatic glucose sensing^a

CME	Reaction method	Determination techniques involved	Linear range (μM to mM)	Sensitivity (μA mM ⁻¹ cm ⁻²)	LOD (μM)	Ref.
g-C ₃ N ₄ /Fe ₂ O ₃ -Cu composite	Non enzymatic	CV, Amp <i>I</i> - <i>t</i>	0.6–2.0	—	0.3	57
Bulk Ni	Non enzymatic	CV, EIS, CA, Amp <i>I</i> - <i>t</i>	0.5 to 4	2900	13	30
g-C ₃ N ₄ nanosheets	Enzymatic	CV, EIS, Amp <i>I</i> - <i>t</i>	50–2	21.7	5	40
3D Ni ₃ S ₂ nanosheets/Ni foam	Non enzymatic	CV, EIS, CA, Amp <i>I</i> - <i>t</i>	0.005–3.0	6148.0	1.2	31
Ni ₃ S ₂ /carbon nanotube	Non enzymatic	CV, EIS, CA, Amp <i>I</i> - <i>t</i>	30 to 0.5	345	1	58
g-C ₃ N ₄ nanosheets	Non enzymatic	CV, EIS, Amp <i>I</i> - <i>t</i>	1 to 12	—	11	32
NiS/rGO nanohybrid	Non enzymatic	CV, LSV, Amp <i>I</i> - <i>t</i>	50–1.7	—	10	59
PVP-NiS	Non enzymatic	CV, DPV, Amp <i>I</i> - <i>t</i>	0.2–2.97	1013.76	4.6	60
Au-NiCo ₂ O ₄ /Ni foam	Non enzymatic	CA, Amp <i>I</i> - <i>t</i>	0.005–0.045	44.86	2.64	26
Hierarchical Ni ₃ S ₂ electrode	Non enzymatic	CV, EIS, Amp <i>I</i> - <i>t</i>	0.0005–3	16 460	0.82	33
NiS/S-g-C ₃ N ₄	Non enzymatic	CV, LSV, Amp <i>I</i> - <i>t</i>	0.1 to 2.1	80	1.5	This work

^a CME – chemically modified electrode; CB – carbon black; NiS – nickel sulfide; CV – cyclic voltammetry; Amp *I*-*t* – amperometry; g-C₃N₄ – graphitic carbon nitride; Fe₂O₃ – iron oxide; Cu – copper; Ni – nickel; CA – chronoamperometry; EIS – electrochemical impedance spectroscopy; Au-NiCo₂O₄/Ni – gold-nickel cobalt oxide/nickel; Ni₃S₂ – nickel sulfide; rGO – reduced graphene oxide; PVP – polyvinylpyrrolidone; DPV – differential pulse voltammetry; LSV – linear sweep voltammetry.



where D represents the diffusion coefficient ($\text{cm}^2 \text{s}^{-1}$), n , c , F , A and i are the number of electrons transferred, the bulk concentration of glucose (mol cm^{-3}), Faraday constant, surface area of GCE and the current controlled by the diffusion of glucose from the bulk solution to the electrode/solution interface.^{55,56} On substituting the corresponding values into the Cottrell equation, the diffusion coefficient of glucose was calculated as $6.54 \times 10^{-10} \text{ cm}^2 \text{s}^{-1}$.

Table 1 summarizes a comparison of different electrochemical enzyme-less sensors using graphitic nitride and nickel sulfide based combinations for glucose sensing that indicated that the developed NiS/S-g-C₃N₄ sensor shows similar sensitivity and selectivity to previously reported materials.

Selectivity is an important property in sensor development for practical applications. The anti-interference effect with other common interfering chemicals present in the serum constituents was tested with glucose. Amperometric measurements were used to monitor the selective detection of glucose (200 μM) in the presence of important biomolecules (20 μM) like ascorbic acid, dopamine, uric acid, lactose, and sucrose, and metal ions like magnesium (Mg^{2+}) and calcium (Ca^{2+}) (400 μM). The glucose detection by amperometric signal was not significantly impacted in the presence of interfering compounds. The obtained current values for the interference compounds are given in the bar diagram in Fig. 7. This clearly shows the good selectivity of the present modified electrode. Further, the reproducibility of the present sensor was evaluated by amperometric measurements using the NiS/S-g-C₃N₄ modified GC electrode. The reproducibility of the measurement was verified by fabricating four different NiS/S-g-C₃N₄ modified electrodes and checking their glucose response (300 μM). The current deviation for the four electrodes is 4.4%, indicating that the present electrode fabrication and the glucose detection procedure are highly reproducible (Fig. S7†). The stability of the sensor was also checked by measuring the oxidation peak current density towards 300 μM glucose after 7 days. The current response was observed to decrease only to 92.77% after

7 days of storage, clearly indicating that the developed sensor system is highly stable (Fig. S8†).

4. Conclusion

The present work demonstrated a simple and modest electrode fabrication for the non-enzymatic electrochemical sensing of glucose with nickel sulfide and sulfur-doped graphitic carbon nitride (NiS/S-g-C₃N₄) in a 0.1 M NaOH medium. The NiS/S-g-C₃N₄ nanohybrid material was prepared by a simple single-step pyrolysis method. The morphological study reveals that the successful incorporation of NiS nanoparticles on the S-g-C₃N₄ nanosheet surface benefits the sensor electrode by promoting electrocatalytic processes and electrical conductivity. In order to show the enhanced electrocatalytic behavior of glucose, the LSV technique was utilized in which a linear increase in the anodic peak current due to glucose oxidation was observed. The prepared NiS/S-g-C₃N₄ nanohybrid material was utilized in glucose sensing and showed a limit of detection of 1.5 μM (S/N = 3) with a sensitivity of 80 $\mu\text{A mM}^{-1} \text{cm}^{-2}$ and the response time of the fabricated sensor was close to 5 s. The presence of inorganic ions and organic substances did not interfere with the glucose sensing. Other biosensor requirement studies and the test results were also satisfactory. The NiS/S-g-C₃N₄ nanohybrid material could expand the various opportunities of the electrochemical sensing of glucose.

Conflicts of interest

The authors declare no competing financial interest.

Acknowledgements

Dr A. Pandikumar thanks DST-SERB, New Delhi for the financial support through Early Career Research (ECRA) Award (SERB File No.: ECR/2017/001758). Mr S. Vinoth and Dr K. S. Shalini Devi are recipients of DST-Inspire Fellowship (IF170687) and DST-SERB National Post-Doctoral Fellowship (PDF/2019/001764), respectively. The financial support from the DST-Inspire faculty award is gratefully acknowledged by Dr S. Radhakrishnan (DST/INSPIRE/04/2015/002259). The authors thank CIF, CSIR-CECRI for the instrument facilities.

References

- 1 J. Wang, *Chem. Rev.*, 2008, **108**, 814–825.
- 2 J. Gonzalo-Ruiz, M. Asunción Alonso-Lomillo and F. Javier Muñoz, *Biosens. Bioelectron.*, 2007, **22**, 1517–1521.
- 3 J. C. Pickup, F. Hussain, N. D. Evans, O. J. Rolinski and D. J. S. Birch, *Biosens. Bioelectron.*, 2005, **20**, 2555–2565.
- 4 M. S. Steiner, A. Duerkop and O. S. Wolfbeis, *Chem. Soc. Rev.*, 2011, **40**, 4805–4839.
- 5 J. Luo, P. Luo, M. Xie, K. Du, B. Zhao, F. Pan, P. Fan, F. Zeng, D. Zhang, Z. Zheng and G. Liang, *Biosens. Bioelectron.*, 2013, **49**, 512–518.
- 6 D. Li, J. Wu, P. Wu, Y. Lin, Y. Sun, R. Zhu, J. Yang and K. Xu, *Sens. Actuators, B*, 2015, **213**, 295–304.

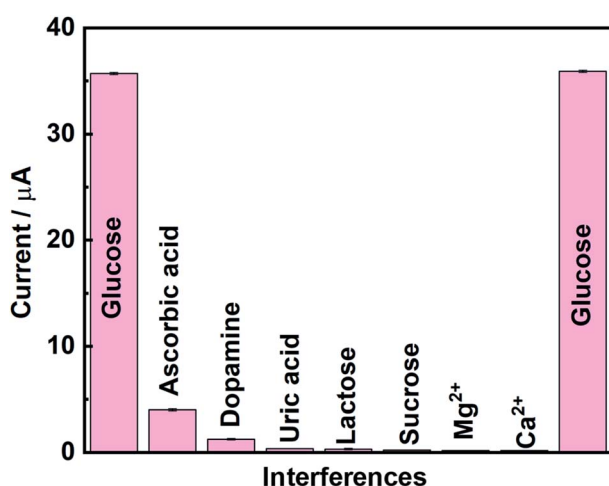


Fig. 7 Selectivity studies using the NiS/S-g-C₃N₄ modified electrode with various interference compounds.



- 7 Y. Z. Wang, H. Zhong, X. R. Li, G. Q. Liu, K. Yang, M. Ma, L. L. Zhang, J. Z. Yin, Z. P. Cheng and J. K. Wang, *Sens. Actuators, B*, 2016, **230**, 449–455.
- 8 A. Heller and B. Feldman, *Chem. Rev.*, 2008, **108**, 2482–2505.
- 9 J. Wu and F. Yin, *J. Electroanal. Chem.*, 2013, **694**, 1–5.
- 10 P. Si, Y. Huang, T. Wang and J. Ma, *RSC Adv.*, 2013, **3**, 3487–3502.
- 11 J. Li and X. Lin, *Biosens. Bioelectron.*, 2007, **22**, 2898–2905.
- 12 B. Wu, G. Zhang, S. Shuang and M. M. F. Choi, *Talanta*, 2004, **64**, 546–553.
- 13 K. Han, Z. Wu, J. Lee, I. S. Ahn, J. W. Park, B. R. Min and K. Lee, *Biochem. Eng. J.*, 2005, **22**, 161–166.
- 14 T. J. Ohara, R. Rajagopalan and A. Heller, *Anal. Chem.*, 1994, **66**, 2451–2457.
- 15 F. Kurniawan, V. Tsakova and V. M. Mirsky, *Electroanalysis*, 2006, **18**, 1937–1942.
- 16 Y. Mu, D. Jia, Y. He, Y. Miao and H. L. Wu, *Biosens. Bioelectron.*, 2011, **26**, 2948–2952.
- 17 Y. Ding, Y. Wang, L. Su, M. Bellagamba, H. Zhang and Y. Lei, *Biosens. Bioelectron.*, 2010, **26**, 542–548.
- 18 C. Li, Y. Su, S. Zhang, X. Lv, H. Xia and Y. Wang, *Biosens. Bioelectron.*, 2010, **26**, 903–907.
- 19 X. M. Chen, Z. J. Lin, D. J. Chen, T. T. Jia, Z. M. Cai, X. R. Wang, X. Chen, G. N. Chen and M. Oyama, *Biosens. Bioelectron.*, 2010, **25**, 1803–1808.
- 20 R. A. Soomro, O. P. Akyuz, R. Ozturk and Z. H. Ibupoto, *Sens. Actuators, B*, 2016, **233**, 230–236.
- 21 I. H. Yeo and D. C. Johnson, *J. Electroanal. Chem.*, 2000, **484**, 157–163.
- 22 C. Barrera, I. Zhukov, E. Villagra, F. Bedioui, M. A. Pérez, J. Costamagna and J. H. Zagal, *J. Electroanal. Chem.*, 2006, **589**, 212–218.
- 23 L. Özcan, Y. Şahin and H. Türk, *Biosens. Bioelectron.*, 2008, **24**, 512–517.
- 24 K. Wang, J. J. Xu and H. Y. Chen, *Biosens. Bioelectron.*, 2005, **20**, 1388–1396.
- 25 P. Kannan, F. Chen, H. Jiang, H. Wang, R. Wang, P. Subramanian and S. Ji, *Analyst*, 2019, **144**, 4925–4934.
- 26 K. K. Naik, A. Gangan, B. Chakraborty and C. S. Rout, *Analyst*, 2018, **143**, 571–579.
- 27 Z. H. Ibupoto, A. Nafady, R. A. Soomro, Sirajuddin, S. T. Hussain Sherazi, M. I. Abro and M. Willander, *RSC Adv.*, 2015, **5**, 18773–18781.
- 28 X. Luo, M. Huang, D. He, M. Wang, Y. Zhang and P. Jiang, *Analyst*, 2018, **143**, 2546–2554.
- 29 I. Gualandi, Y. Vlamidis, L. Mazzei, E. Musella, M. Giorgetti, M. Christian, V. Morandi, E. Scavetta and D. Tonelli, *ACS Appl. Nano Mater.*, 2019, **2**, 143–155.
- 30 X. Niu, M. Lan, H. Zhao and C. Chen, *Anal. Chem.*, 2013, **85**, 3561–3569.
- 31 H. Huo, Y. Zhao and C. Xu, *J. Mater. Chem. A*, 2014, **2**, 15111–15117.
- 32 J. Tian, Q. Liu, C. Ge, Z. Xing, A. M. Asiri, A. O. Al-Youbi and X. Sun, *Nanoscale*, 2013, **5**, 8921–8924.
- 33 S. Kim, S. H. Lee, M. Cho and Y. Lee, *Biosens. Bioelectron.*, 2016, **85**, 587–595.
- 34 Y. J. Yang, J. Zi and W. Li, *Electrochim. Acta*, 2014, **115**, 126–130.
- 35 L. Liu, H. Lv, C. Wang, Z. Ao and G. Wang, *Electrochim. Acta*, 2016, **206**, 259–269.
- 36 H. Zhang, Q. Huang, Y. Huang, F. Li, W. Zhang, C. Wei, J. Chen, P. Dai, L. Huang, Z. Huang, L. Kang, S. Hu and A. Hao, *Electrochim. Acta*, 2014, **142**, 125–131.
- 37 Y. Zhang, X. Bo, A. Nsabimana, C. Luhana, G. Wang, H. Wang, M. Li and L. Guo, *Biosens. Bioelectron.*, 2014, **53**, 250–256.
- 38 J. Tian, Q. Liu, C. Ge, Z. Xing, A. M. Asiri, A. O. Al-Youbi and X. Sun, *Nanoscale*, 2013, **5**, 8921–8924.
- 39 M. Sadhukhan and S. Barman, *J. Mater. Chem. A*, 2013, **1**, 2752–2756.
- 40 K. J. Tian, H. Liu, Y. P. Dong, X. F. Chu and S. B. Wang, *Colloids Surf., A*, 2019, **581**, 123808.
- 41 P. K. Kannan and C. S. Rout, *Chem.–Eur. J.*, 2015, **21**, 9355–9359.
- 42 S. Vinoth, P. M. Rajaitha and A. Pandikumar, *Compos. Sci. Technol.*, 2020, **195**, 108192.
- 43 M. H. Vu, M. Sakar, C. C. Nguyen and T. O. Do, *ACS Sustainable Chem. Eng.*, 2018, **6**, 4194–4203.
- 44 B. Jansi Rani, N. Dhivya, G. Ravi, S. S. Zance, R. Yuvakkumar and S. I. Hong, *ACS Omega*, 2019, **4**, 10302–10310.
- 45 H. Sha, Y. Zhang, Y. Wang, H. Ke, X. Xiong and N. Jia, *Biosens. Bioelectron.*, 2019, **124–125**, 59–65.
- 46 H. Zhao, H. Yu, X. Quan, S. Chen, Y. Zhang, H. Zhao and H. Wang, *Appl. Catal., B*, 2014, **152–153**, 46–50.
- 47 M. Jourshabani, Z. Shariatnia, G. Achari, C. H. Langford and A. Badiei, *J. Mater. Chem. A*, 2018, **6**, 13448–13466.
- 48 S. Vinoth, P. Sampathkumar, K. Giribabu and A. Pandikumar, *Ultrason. Sonochem.*, 2019, 104855.
- 49 S. Vinoth, R. Ramaraj and A. Pandikumar, *Mater. Chem. Phys.*, 2020, **245**, 122743.
- 50 K. Wang, Q. Li, B. Liu, B. Cheng, W. Ho and J. Yu, *Appl. Catal., B*, 2015, **176–177**, 44–52.
- 51 M. B. Zakaria, C. Li, Q. Ji, B. Jiang, S. Tominaka, Y. Ide, J. P. Hill, K. Ariga and Y. Yamauchi, *Angew. Chem.*, 2016, **128**, 8566–8570.
- 52 J. Wen, X. Li, H. Li, S. Ma, K. He, Y. Xu, Y. Fang, W. Liu and Q. Gao, *Appl. Surf. Sci.*, 2015, **358**, 204–212.
- 53 P. K. Sonkar, V. Ganesan, S. A. John, D. K. Yadav and R. Gupta, *RSC Adv.*, 2016, **6**, 107094–107103.
- 54 J. Li and X. Lin, *Sens. Actuators, B*, 2007, **126**, 527–535.
- 55 B. Dinesh, K. S. Shalini Devi and U. M. Krishnan, *ACS Appl. Bio Mater.*, 2019, **2**, 1740–1750.
- 56 J. Li, H. Xie and L. Chen, *Sens. Actuators, B*, 2011, **153**, 239–245.
- 57 L. Liu, M. Wang and C. Wang, *Electrochim. Acta*, 2018, **265**, 275–283.
- 58 T. W. Lin, C. J. Liu and C. S. Dai, *Appl. Catal., B*, 2014, **154–155**, 213–220.
- 59 S. Radhakrishnan and S. J. Kim, *RSC Adv.*, 2015, **5**, 44346–44352.
- 60 S. Jana, G. Mondal, B. C. Mitra, P. Bera, B. Chakraborty, A. Mondal and A. Ghosh, *New J. Chem.*, 2017, **41**, 14985–14994.

